Signatures of antibonding hole ground states in exciton spectra of vertically coupled quantum dots in an electric field

T. Chwiej and B. Szafran
Faculty of Physics and Applied Computer Science, AGH University of Science and Technology, al. Mickiewicza 30, 30-059 Kraków, Poland

(Received 2 November 2009; revised manuscript received 23 December 2009; published 2 February 2010)

We study exciton energy spectra in a pair of vertically coupled self-assembled quantum dots in external electric field. We perform a systematic comparison of the four-band Luttinger Kohn modeling producing an antibonding hole ground state with the single valence-band approximation in which the hole ground state has the bonding character. We find that the single-band approximation remains relevant for description of the electric field dependence of the photoluminescence spectrum for interdot barrier thickness of 7 nm or larger. We explain that for thinner barriers the antibonding character of the hole orbital can be deduced from the ground state recombination probability as a function of the electric field.

DOI: 10.1103/PhysRevB.81.075302 PACS number(s): 73.21.La, 73.43.−f, 71.10.Pm

I. INTRODUCTION

Self-assembled InGaAs/GaAs quantum dots spontaneously grow in stacks[1] and the photoluminescence (PL) spectra measurements performed more than a decade ago indicated that confined carriers form extended states within the stack due to the interdot tunnel coupling.[1,2] A detailed experimental study of these artificial molecular orbitals for a single pair of quantum dots placed in an external electric field was realized only several years later.[3,4] Since then, the PL experiments[5] on artificial molecules in electric field provided a large number of data on the role of Coulomb and spin-related interactions as well as on the nature of the interdot tunneling.

The lowest-energy hole states confined in quantum dots can be nearly entirely identified with the heavy hole valence band.[6] This fact is usually used as an argument for the single-band modeling as the first approximation for the description of the low-energy hole states. The single-band modeling for the interdot barrier thickness of about 6 to 10 nm turned out to be quite successful in determination of the features of the PL spectra related to the electron tunneling between the dots. In particular Ref. 7 correctly predicted the optical signatures of the electric field-induced exciton dissociation by avoided crossings of the direct and indirect exciton energy levels as observed in a parallel experimental work.[3] Moreover PL signatures of the negative trion dissociation related to the removal of electrons from the dot occupied by the hole as described in Ref. 7 was precisely confirmed in a subsequent experiment.[8]

The electron interdot tunnel coupling for a pair of identical dots results in formation of a bonding ground state orbital and an antibonding excited orbital. The interdot tunnel coupling for the heavy hole as described by the single-band model is qualitatively similar although weaker. However, it was recently demonstrated[9] that the hole as treated by four-band Luttinger Kohn[10] (KL) Hamiltonian actually forms an antibonding ground state. The reason is that the $k\cdot p$ Hamiltonian does not commute with the spatial parity operator. The light hole tunnels more effectively than the heavy hole and the bonding light hole orbital couples to the antibonding heavy hole state. Even a small contribution of the bonding light hole orbital triggers formation of a ground state which is predominantly related to the antibonding heavy hole orbital.[9] A signature of the antibonding character of the heavy hole ground state was indeed found[11] in the Zeeman shifts of the PL lines from which the penetration of the hole to the GaAs tunnel barrier can be deduced.

Although the experiment[11] was performed in external electric field, the theoretical calculations that form the basis for the present understanding of the interdot hole tunnel coupling[9,12] were performed with a neglect of the electric field. In the present paper we study the exciton energies as well as carrier recombination probabilities in function of the external electric field to determine signatures of the antibonding hole ground state that could be extracted directly from the electric field dependence of the low-energy PL spectrum in the absence of the external magnetic field. For that purpose we compare the results as obtained by the four-band hole modeling—which produces the antibonding hole ground state—to the ones given by the single heavy hole band approximation—in which the hole ground state has the bonding character.

Formation of the antibonding hole ground state for identical quantum dots[9] is due to the energy resonance appearing for both the heavy and light hole states confined in separate dots. The pairs of vertically coupled quantum dots are never identical[1] and additional confinement asymmetry can be intentionally introduced[14,15] by specific growth conditions. The asymmetry in the quantum dots potential may be to an extent compensated by the electric field, but the antibonding hole state can appear only provided that resonance for the heavy and light hole states is achieved for the same value of the electric field. In this paper we provide a systematic study of the asymmetry effects for optical signatures of the antibonding hole ground state. We find that the exciton energy spectra as calculated by the four-band Hamiltonian and by the heavy hole approximation become similar for strongly asymmetric dots. Nevertheless the ground state recombination probabilities as obtained by the two approaches remain very different for the electric fields which induce the hole transfer between the dots.

 ©2010 The American Physical Society

II. THEORY

We consider an electron-hole pair in the two vertically stacked InGaAs quantum dots. The dots are considered ideally circular, coaxial and with identical radius $R=10$ nm (following Ref. 9). The confinement potential is taken in a separable form $V(\rho,z)=V_r(\rho)+V_z(z)$, where the z axis is identified with the rotational symmetry axis of the system. In the present work we adopt an infinite potential well for the radial potential V_r which dot not perturb the essential physics of the interdot coupling along the axis of the stack. For the vertical confinement we adopt a double finite potential well resulting from the conduction and valence-band offsets of depth $V^e=380$ meV for electrons and $V^h=530$ meV for the holes.[9] The height of the lower dot is assumed equal[9] to $h_1=2.0$ nm and the height of the upper one is taken between $h_2=2.0$ nm and $h_2=2.5$ nm. The external electric field is assumed parallel to the z axis ($\vec{F}=[0,0,F]$).

We consider the following Hamiltonian for the interacting electron-hole pair

$$\hat{H}_{eh}=\hat{H}_h+\hat{H}_e+\hat{V}_{eh}, \tag{1}$$

where $\hat{H}_h$ and $\hat{H}_e$ are the hole and the electron Hamiltonians while the term $\hat{V}_{eh}=-1/(\epsilon r_{eh})$ is responsible for their Coulomb interaction (equations are written in atomic units and the dielectric constant is taken equal to $\epsilon=12.9$). We neglect the electron-hole exchange interaction as small at the energy scale of the avoided crossings observed at the exciton dissociation. The exchange energy estimated for vertically coupled dots by application of the transverse magnetic field mixing the dark and bright exciton states[13] is about 0.25 meV.

The KL (Refs. 9, 10, 12, and 16) Hamiltonian describes the degenerate two light and two heavy hole bands corresponding to angular momentum $j=\frac{3}{2}$. The split-off hole band ($j=\frac{1}{2}$) is neglected in the Hamiltonian, since it lies at least 200 meV below the top of the valence band. We use the KL Hamiltonian in its conventional form

$$\hat{H}_h=\begin{pmatrix}\hat{P}_+ & \hat{R} & -\hat{S} & 0\\ \hat{R}^* & \hat{P}_- & 0 & \hat{S}\\ -\hat{S}^* & 0 & \hat{P}_- & \hat{R}\\ 0 & \hat{S}^* & \hat{R}^* & \hat{P}_+\end{pmatrix}+(V^h+e\vec{r}\vec{F})\mathbf{I}, \tag{2}$$

where $\vec{r}$ is the hole position vector and $\mathbf{I}$ is the identity matrix. The form of Eq. (2) assumes that the four components of the hole spinor—each related to a different projections of the Bloch angular momentum on the z axis—are put in the order $j_z=+\frac{3}{2}$, $-\frac{1}{2}$, $+\frac{1}{2}$, and $-\frac{3}{2}$, corresponding to the heavy spin up, the light spin down, the light spin up, and the heavy spin-down hole bands, respectively. The operators appearing in the Hamiltonian (2) are defined[10] as

$$\hat{P}_+=\frac{1}{2}[(\gamma_1+\gamma_2)\hat{p}_\perp^2+(\gamma_1-2\gamma_2)\hat{p}_z^2], \tag{3}$$

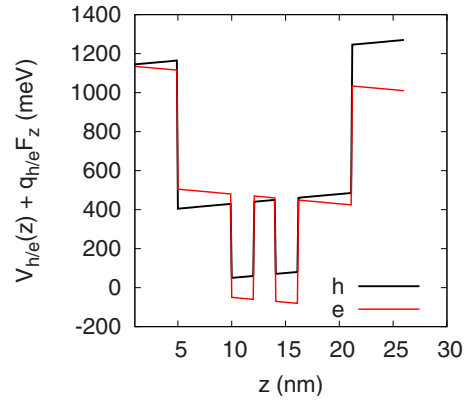

FIG. 1. (Color online) Vertical confinement potential for electron and hole in a pair of identical dots in presence of an electric field of $F=50$ kV/cm applied parallel to the symmetry axis of the system (z).

$$\hat{P}_-=\frac{1}{2}[(\gamma_1-\gamma_2)\hat{p}_\perp^2+(\gamma_1+2\gamma_2)\hat{p}_z^2], \tag{4}$$

$$\hat{R}=\frac{-\sqrt{3}}{2}\gamma_2\hat{p}_-^2, \tag{5}$$

$$\hat{S}=\sqrt{3}\gamma_3\hat{p}_-\hat{p}_z, \tag{6}$$

where $\hat{p}_-=\hat{p}_x-i\hat{p}_y$ and $\hat{p}_\perp^2=\hat{p}_x^2+\hat{p}_y^2$. The Luttinger parameters γ_i appearing in the above equations are taken for the $In_{0.53}Ga_{0.47}As$ alloy:[17] $\gamma_1=11.01$, $\gamma_2=4.18$, and $\gamma_3=4.84$.

The eigenfunctions of the *diagonal* part of operator (2) can be written down in a form

$$\exp(il\phi)\varphi^h_{ijlj_z}(\rho,z)|j_z\rangle=\exp(il\phi)J_l\left(\frac{\alpha_i^l\rho}{R}\right)W_{j|j_z|}(z)|j_z\rangle, \tag{7}$$

where l is the orbital angular momentum, J_l is the Bessel function of the first kind, α_i^l is its i-th root, and $W_{j,|j_z|}$ is the j-th hole eigenstate of the vertical part of the diagonal Hamiltonian

$$\hat{h}_z=-\frac{1}{2m^*_{|j_z|}}\frac{\partial^2}{\partial z^2}+V_h(z)+ezF, \tag{8}$$

in which we use $m^*_{1/2}=1/(\gamma_1+2\gamma_2)$ for the light hole and $m^*_{3/2}=1/(\gamma_1-2\gamma_2)$ for the heavy hole. Operator (8) is diagonalized on a one-dimensional mesh of points with spatial step of $\Delta=0.1$ nm. The potential for the electron and the hole along the axis of the stack is given in Fig. 1 for the electric field $F=50$ kV/cm.

Hamiltonian (2) for a given projection of the total angular momentum on the z axis (m_z) is diagonalized in the basis

$$\psi^h_{m_zn}=\sum_{i,j,j_z}b^{m_zn}_{ijj_z}e^{i(m_z-j_z)\phi}\varphi^h_{ij|m_z-j_z|j_z}(\rho,z)|j_z\rangle, \tag{9}$$

where the normalization of the basis elements is included in the expansion coefficients b. The electron Hamiltonian is also taken in the separable form

$$\hat{H}_e = \hat{h}_{\rho,\phi} + \hat{h}_z \tag{10}$$

where $\hat{h}_{\rho,\phi}$ is the kinetic energy operator and $\hat{h}_z$ is given by Eq. (8) only with an inverse electric charge $-e$ and the electron band mass $m_e^*=0.05$. Each electronic basis state has definite z component of the orbital angular momentum (l) and the spin projection on the z axis ($\sigma=\pm 1/2$)

$$\psi^e_{mkl\sigma} = c_{mkl} e^{il\phi} \varphi^e_{mkl}(\rho,z)|\sigma\rangle = c_{mkl} e^{il\phi} \varphi^e_{mkl\sigma}(\rho,z) \tag{11}$$

where c_{mkl} is the normalization constant, m and k specify the number of radial and vertical excitation, respectively for a given angular momentum l.

The wave function of the exciton is calculated using an exact diagonalization of Hamiltonian (1) in a basis of noncorrelated products of single-particle eigenfunctions

$$\Psi^{exc}_M = \sum A^M_{m_z nmkl\sigma} \psi^h_{m_z n} \psi^e_{mkl\sigma}. \tag{12}$$

We insert into the basis electron eigenfunctions with $l=0$ and ± 1. For each angular momentum we use 16 states with $m,k=1,2,3,4$, which gives in total 48 basis functions. For the hole we use 32 lowest-energy eigenstates of the KL Hamiltonian. The essential point of the calculation is the evaluation of the Coulomb matrix elements for the electron-hole pair

$$\begin{aligned}\langle \Psi_M|\hat{V}_{eh}|\Psi_{M'}\rangle &= \sum A^M_{m_z nmkl\sigma} A^{M'}_{m'_z n' m' k' l' \sigma'} \int d^3\vec{r}_h (\psi^h_{m_z n})^* \psi^h_{m'_z n'} \\ &\times \int d^3\vec{r}_e \frac{1}{\epsilon r_{eh}} (\psi^e_{mkl\sigma})^* \psi^e_{m'k'l'\sigma'}.\end{aligned} \tag{13}$$

After summation over the electron spin degrees of freedom the second integral can be treated simply as the electrostatic potential for the hole generated by the electron,[18]

$$V^{mkl}_{m'k'l'}(\vec{r}_h) = \int d^3\vec{r}_e \frac{1}{\epsilon r_{eh}} (\psi^e_{mkl})^* \psi^e_{m'k'l'}. \tag{14}$$

We solve the Poisson equation for this potential

$$\nabla^2 V^{mkl}_{m'k'l'} = -\frac{4\pi}{\epsilon} [\varphi^e_{mkl}(\rho,z)]^* \varphi^e_{m'k'l'}(\rho,z) e^{i(l'-l)\phi}. \tag{15}$$

The potential adopts the rotational symmetry of the right-hand side of Eq. (15)

$$V^{mkl}_{m'k'l'}(\rho,z,\phi) = V^{mkl}_{m'k'l'}(\rho,z,0) e^{i(l'-l)\phi}. \tag{16}$$

Since the angular form of the potential is given by Eq. (16) the Poisson Eq. (15) can be solved on a two-dimensional mesh. For that purpose we use a finite difference relaxation approach. The nodes of the mesh are defined as $\rho_i = i\Delta_\rho$ and $z_j = j\Delta_z$ with the mesh spacing $\Delta_z=0.1$ nm and $\Delta_\rho=0.083$ nm. For the calculation of the Coulomb matrix elements we need to solve the Poisson equation for all $48^2=2304$ pairs of the electron wave functions that enter the Coulomb integral (13). The adopted procedure[18] is nevertheless much faster than a direct six-dimensional integration of $48^2 \times 32^2$ Coulomb matrix elements. Given the electron potential the Coulomb matrix elements read[19]

$$\begin{aligned}\langle \Psi_M|\hat{V}_{eh}|\Psi_{M'}\rangle &= \sum (A^M_{m_z nmkl\sigma})^* A^{M'}_{m'_z n' m' k' l' \sigma'} \\ &\times \sum (b^{m_z n}_{ijj_z})^* b^{m'_z n'}_{i'j'j'_z} (c_{mkl})^* c_{m'k'l'} \\ &\times \int d\rho dz d\phi \rho (\varphi^h_{ijm_z j_z})^* \varphi^h_{i'j'm'_z j'_z} V^{mkl}_{m'k'l'}(\rho,z,0) \\ &\times e^{i[(m'_z - j'_z)-(m_z - j_z)+(l'-l)]\phi}.\end{aligned} \tag{17}$$

The probability of radiative recombination for the M exciton state is evaluated as proportional to square of the overlap of the electron wave function to the hole spinor elements summed over the valence bands and the electron spin states

$$p_M = \sum_{j_z,\sigma} \delta_{|j_z+\sigma|,1} \left| \sum_{\substack{m_z,n \\ l,m,k}} A^M_{m_z,n,m,k,l,\sigma} \sum_{i,j} b^{m_z,n}_{i,j,j_z} c_{m,k,l} \int d^3\vec{r}_e d^3\vec{r}_h \Phi^h_{i,j,j_z,m_z}(\vec{r}_h) \Phi^e_{m,k,l,0}(\vec{r}_e) \delta(\vec{r}_e - \vec{r}_h) \right|^2, \tag{18}$$

where $\Phi^\beta_{i,j,l_1,l_2}(\vec{r}) = e^{i(l_1-l_2)\phi} \varphi^\beta_{m,k,l_1,l_2}(\rho,z)$ in accordance with Eqs. (7) and (11) and the term $\delta_{|j_z+\sigma|,1}$ is responsible for the spin selection rule.

III. RESULTS

A. Test calculations for the hole

For a pair of identical dots we reproduce the main result of Ref. 9—in the four-band Hamiltonian (2) the antibonding hole ground state is found for the barrier thickness larger than 1.5 nm—see the energy levels presented with the red curves in Fig. 2(a). In the kp calculation, the contribution of the light hole [of about 5%—see Fig. 2(c)] lowers the ground state energy by as much as $\simeq 20$ meV. We also performed calculations in the six-band Luttinger Kohn Hamiltonian including the split-off band given in the Appendix. The split-off valence-band contribution to the hole ground state is of the order of 1% [see Fig. 2(c)]. In the six-band Hamiltonian the contribution of the light hole is slightly reduced and the

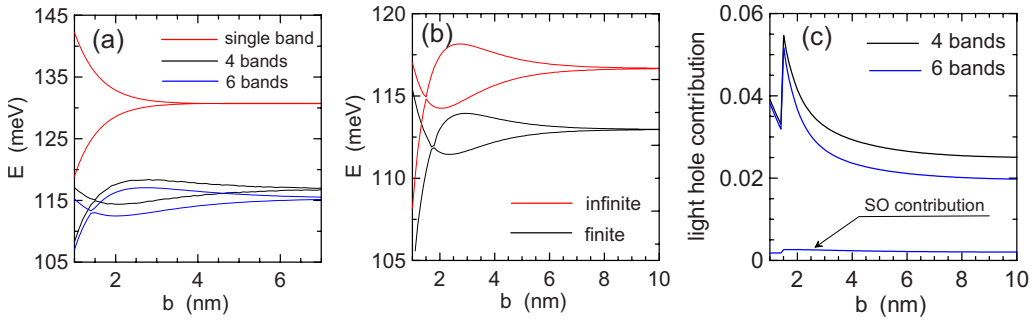

FIG. 2. (Color online) (a) Two lowest-energy levels of the hole for identical pair of quantum dots as calculated in the heavy hole single-band approximation [light gray (red) curves] as function of the interdot barrier thickness b. Black curves show the results obtained in the four-band KL Hamiltonian [Eq. (2)] and dark gray (blue) ones the results of the six-band Hamiltonian given by Eq. (A1). (b) Comparison of the results of the four-band modeling with the assumption of infinite potential well in the radial direction (red curve) and the results obtained in a model of a finite potential disklike quantum well of depth $V^h=530$ meV. (c) Two upper curves show the contribution of the light hole to the ground state wave function as obtained in the four-band modeling (black curve). The contribution of the split-off (SO) valence band in the six-band modeling is also shown.

energy levels [dark gray (blue) curves in Fig. 2(a)] are shifted down by about 1 meV with respect to the four-band modeling. Moreover, we performed calculations in a finite disk quantum well model of depth V_h. The results as obtained by the imaginary time technique[20] are compared with the infinite radial well model in Fig. 2(b). For the finite quantum well the energy levels are shifted down by about 5 meV and the energy splitting between the bonding and antibonding states is slightly reduced. We conclude that the both inclusion of the split-off band and account taken for the finite depth of the radial potential introduce no qualitative difference for the description of the splitting of the bonding and antibonding energy levels, which is therefore adopted in the following.

B. Exciton spectra for identical dots

We begin the discussion of the exciton spectra in the electric field by the ideal case of identical dots for which the contribution of the light hole is expected to be the strongest. Comparison of the exciton energy spectra as obtained with the KL Hamiltonian and in the heavy hole approximation is given in Fig. 3 (the energies are given with respect to the

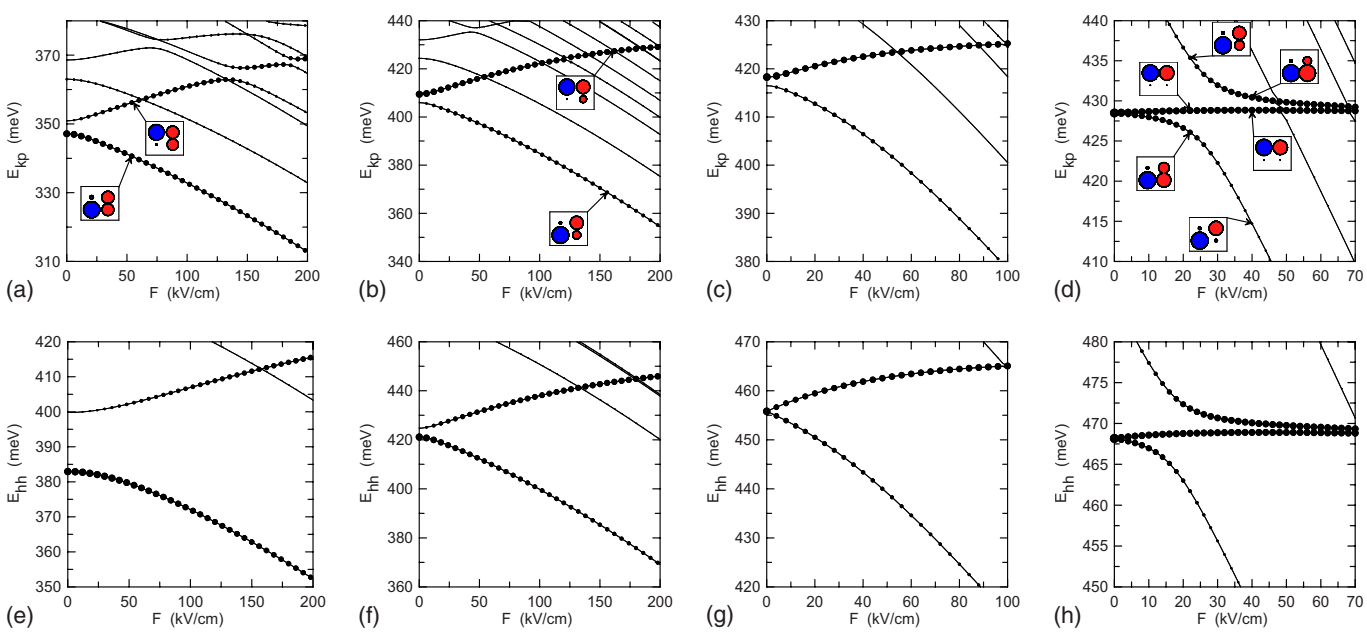

FIG. 3. (Color online) Energy spectrum for a pair of identical dots in function of the electric field. The interdot barrier thickness b =1.2, 2.1, 4.1, and 7 nm is assumed in panels (a) and (e), (b) and (f), (c) and (g), and (d) and (h), respectively. Radius of the circles is set proportional to the recombination probability. The upper row of plots was obtained with the four-band description of the hole, and the lower row of plots by the heavy hole approximation. The insets in (a), (b), and (d) show the charge distribution of the carriers in the two dots. The areas of the circles is proportional to the electron (the right pair of circles) and hole (the left pair of circles) charge accumulated in the lower dot (the lower pair of circles) and in the upper dot (the upper pair of circles).

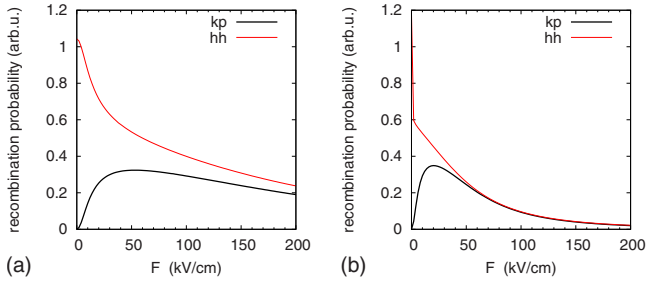

FIG. 4. (Color online) Ground state recombination probability for a pair of identical dots separated by the barrier of (a) $b=2.1$ nm and (b) $b=4.1$ nm. Black curves show the results obtained with the kp method and the red lines by the heavy hole model.

energy gap of the dot material). The electron tunnel coupling between the dots for $b=7$ nm—the thickest of the interdot barrier considered here—results in the avoided crossing between the ground state and the second optically active energy level that is observed in Figs. 3(d) and 3(h). The states that participate in the avoided crossing (ground state and the second-excited energy levels) correspond to the hole localized in the lower dot (see the insets to the figure which indicate the electron and the hole distributions), and the avoided crossing is related to the ground state removal of the electron to the upper dot which is accompanied by vanishing ground state recombination probability due to separation of the carriers.[7] The light hole tunnels between the dots as effectively as the electron. Therefore one could expect that the energy spectra for the heavy hole and kp modeling should be different already for this value of the barrier thickness. However, this is not observed. Figures 3(d) and 3(h) show that the pattern of optically active energy levels as calculated by the four-band model is qualitatively identical to the results of the heavy hole approximation.

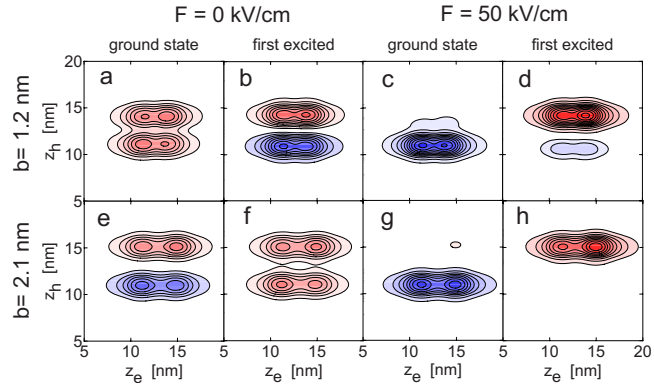

FIG. 5. (Color online) Ground state and first-excited state wave functions plotted on the axis of the stack for $\rho_e=\rho_h=0$ for a pair of identical dots separated by the barrier of (a)–(d) $b=2.1$ nm and (e)–(h) $b=4.1$ nm for $F=0$ and $F=50$ kV/cm. The horizontal (vertical) axes correspond to the electron (heavy hole) z coordinate. Red and blue colors correspond to opposite signs of the wave functions.

For the detection of the spectral features due to the antibonding hole orbital we consider smaller values of interdot barrier thickness. For $b=4.1$ and 2.1 nm [Figs. 3(b), 3(c), 3(f), and 3(g)] the optically active energy levels in both calculation vary with the electric field in a similar manner. More pronounced is the difference in the ground state recombination probability (RP), which was plotted in Figs. 4(a) and 4(b). In the heavy hole model we notice an abrupt drop of RP when the electric field is applied. This is due to the mixing of nearly degenerate antibonding and bonding states by the field.

The reason behind the drastically different RP dependence as obtained by the KL and single-band modeling can be understood by considering the heavy hole component of the exciton wave function plotted in Fig. 5 along the symmetry axis of the system $[\rho_e=\rho_h=0]$. For $b=2.1$ nm and $F=0$ the

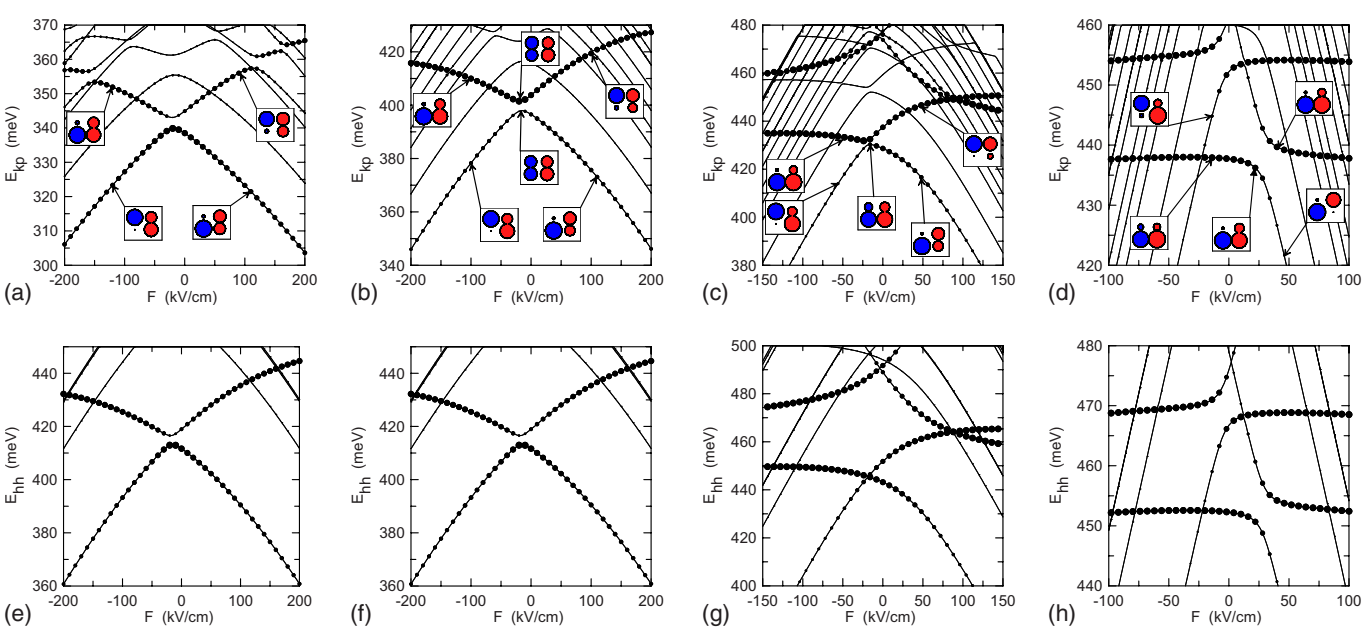

FIG. 6. (Color online) Same as Fig. 3 but for a slightly asymmetric pair of quantum dots, the lower one has height $h_l=2$ nm and the upper $h_u=2.1$ nm.

ground state wave function has nodal surfaces (changes sign) along the hole coordinate which results from the antibonding hole orbital. The electron-hole correlation is evident in the localization of the extrema of the wave function on the diagonal of the plot $z_e = z_h$ which corresponds to electron and hole remaining in the same position. In the calculation of RP one integrates the exciton wave function for $\mathbf{r}_e = \mathbf{r}_h$, which in the context of Fig. 5 corresponds to integration over the diagonal. The resulting integral is zero due to the nodal surface present in the ground state. For $F = 50$ kV/cm the ground state wave functions corresponds to the hole nearly completely localized in the lower dot and the electron present in both the dots. Still a trace of the hole presence in the upper dot can be seen [Fig. 5(g)]. The ground state wave function still changes sign along the diagonal of the plot, but the integral of the wave function over the diagonal is no longer zero due to the imbalance of the carrier distribution between the dots introduced by the electric field.

For $b = 1.2$ nm the hole ground state as obtained by the KL modeling becomes bonding [see Fig. 2(a)]. For that barrier thickness the heavy hole tunneling is finally activated and the effect dominates over the light hole tunneling due to the larger contribution of the heavy hole band. For the bonding hole ground state the RP becomes a monotonic function of F as in the heavy hole approximation [see Figs. 3(a) and 3(e)]. Figure 4 shows that at higher field the RPs in both kp and heavy hole calculations become identical, which is consistent with the plots of the wave functions given in Figs. 5(c), 5(d), 5(g), and 5(h) which are similar for both $b = 1.2$ and 2.1 nm.

We conclude that at the center of the avoided crossing related to the hole switching between the dots, the electron-hole recombination probability is minimal for the antibonding hole orbital and maximal for the hole in the bonding state.

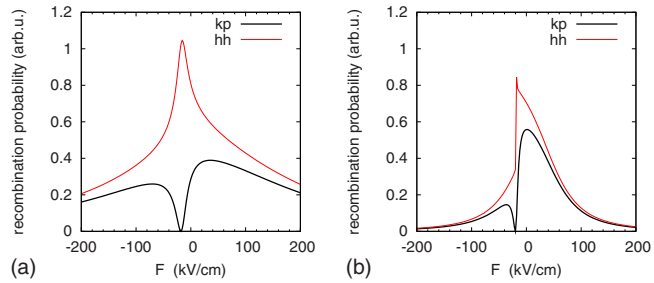

FIG. 7. (Color online) Same as Fig. 4 but for the pair of nonidentical dots $h_l = 2$ nm, $h_u = 2.1$ nm. Barrier thickness $b = 2.1$ nm is applied in (a) and $b = 4.1$ nm in (b).

C. Nonidentical dots

The striking difference of the RP probabilities as found above for the bonding and antibonding hole ground states can only be useful in an experiment provided that similar features are found for nonidentical dots. In order to verify this point we introduced an asymmetry to the system by increasing the height of the upper dot.

For a small asymmetry—the height of the upper dot increased from 2 to 2.1 nm and in the strong coupling limit [Figs. 6(a) and 6(e)] the extrema of the energy levels are shifted to the negative electric field. In Figs. 6(b) and 6(f) we notice that although the two lowest-energy levels enter into similar avoided crossing in both kp and single-band calculations, the RPs for these levels are inverted. In Fig. 7 we can see that the ground state RP drops to zero at the center of the avoided crossing in the kp calculation. This indicates that the ground state hole state becomes orthogonal to the bonding electron state, i.e., the heavy hole $l = 0$ spinor acquires an antibonding character at the center of the avoided crossing, in contrast to the heavy hole modeling for which the recombination probability is maximal at the avoided crossing. The

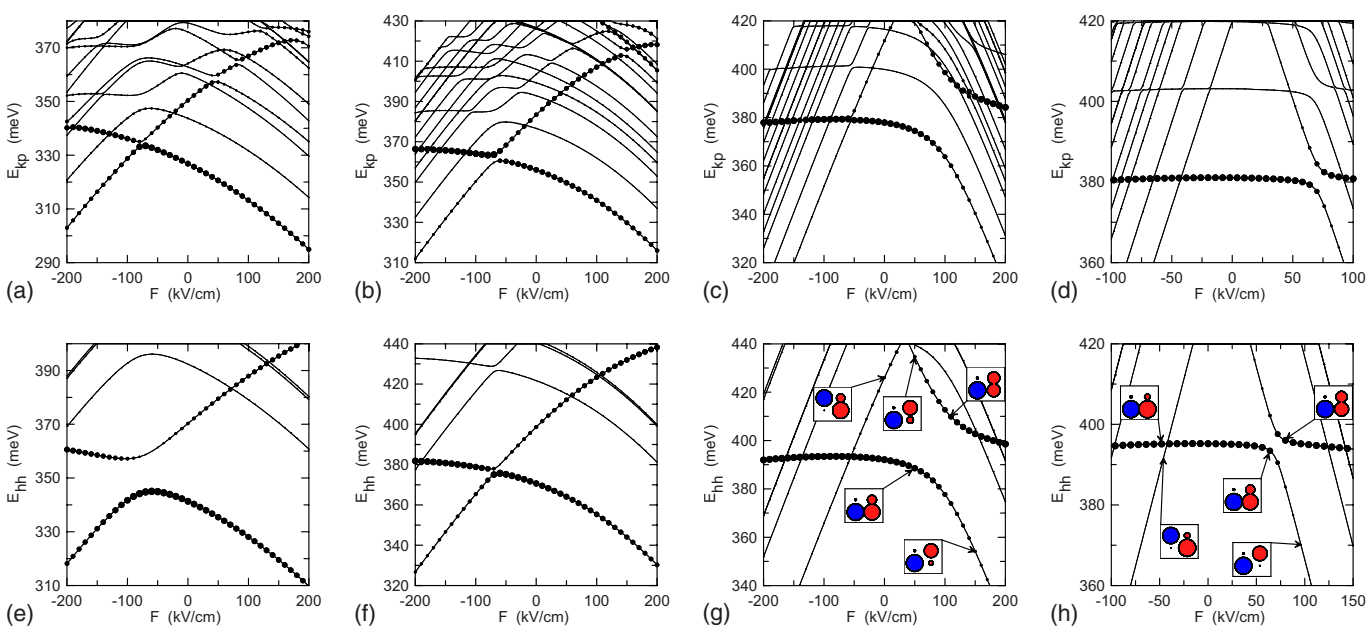

FIG. 8. (Color online) Same as Fig. 3 but for strongly asymmetric pair of quantum dots, the lower one has height $h_l = 2$ nm and the upper $h_u = 2.5$ nm.

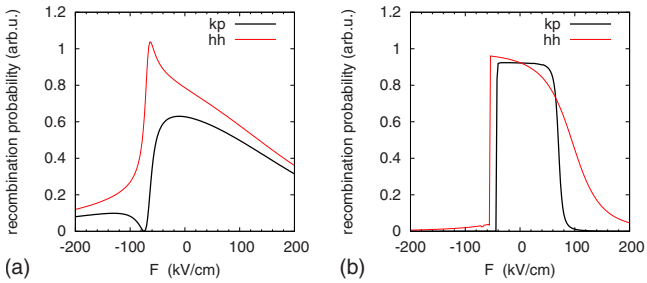

FIG. 9. (Color online) Same as Fig. 4 but for the pair of nonidentical dots $h_l=2$ nm, $h_u=2.5$ nm. Barrier thickness $b=2.1$ nm is applied in (a) and $b=4.1$ nm in (b).

ground state avoided crossings observed in Figs. 6(a)–6(c) are related to the hole transfer between the dots. For larger barrier thickness [Fig. 6(d)] the ground state avoided crossing related to the hole transfer become too narrow to be noticed at the energy scale applied in the figure. The ground state RP dependence on the field becomes similar in both approaches [Fig. 7(b)], still only the one obtained by the kp method drops to zero at the center of avoided crossing. The ground state avoided crossing that for $b=7$ nm is clearly seen near +40 kV/cm in Figs. 6(d) and 6(h) is due to the electron transfer. In this case the results of both methods for the optically active energy levels are identical. This electron transfer related avoided crossing—of an indirect exciton energy level (separated carriers) with the direct one (carriers in the same dot) was historically the first optical signature reported experimentally in Ref. 3 and found in the heavy hole modeling of Ref. 7.

For strongly asymmetric dots [Figs. 8 and 9] the features of the optically active states as obtained by the single-band model and by the kp method are identical for $b>4$ nm. However, for $b=2.1$ nm [Figs. 8(b), 8(f), and 9] the ground state RP as calculated by the multiband approach distinctly drops to zero at the hole transfer-related avoided crossing, while the single-band modeling produces a maximal RP.

IV. SUMMARY AND CONCLUSIONS

We have performed an exact diagonalization study of exciton spectra and electron-hole recombination probabilities for a pair of symmetric and asymmetric quantum dots in the presence of external electric field. We demonstrated that the heavy hole modeling correctly describes the spectral consequences of the electron transfer between the dots. The single-band modeling is therefore relevant for the interdot coupling for barrier thickness of about 7 nm or larger. We also indicated that the antibonding character of the heavy hole orbital for barrier thickness between $\simeq 2$ and $\simeq 4$ nm can be deduced from the intensity of the lowest-energy PL lines. The recombination probability drops to zero when an antibonding hole ground state is formed at the center of avoided crossing related to the hole transfer between the dots. The electric field dependence of the ground state recombination probability can be used as a measure for probing the type of hybrydization of the ground state hole orbital in artificial molecules.

ACKNOWLEDGMENTS

This work was supported by the AGH UST project No. 11.11.220.01 "Basic and applied research in nuclear and solid state physics." Calculations were performed in ACK–CYFRONET–AGH on the RackServer Zeus.

APPENDIX

For the purpose of Fig. 2(a) we used the following[21] six-band generalization of the hole Hamiltonian (2), including the split-off band

$$H_6 = \begin{pmatrix} \hat{P}_+ & \hat{R} & -\hat{S} & 0 & -\frac{1}{\sqrt{2}}\hat{S} & \sqrt{2}\hat{R} \\ \hat{R}^* & \hat{P}_- & 0 & \hat{S} & \sqrt{\frac{3}{2}}\hat{S}^* & \sqrt{2}\hat{Q} \\ -\hat{S}^* & 0 & \hat{P}_- & \hat{R} & -\sqrt{2}\hat{Q} & \sqrt{\frac{3}{2}}\hat{S} \\ 0 & \hat{S}^* & \hat{R}^* & \hat{P}_+ & -\sqrt{2}\hat{R}^* & -\frac{1}{\sqrt{2}}\hat{S}^* \\ -\frac{1}{\sqrt{2}}\hat{S}^* & \sqrt{\frac{3}{2}}\hat{S} & -\sqrt{2}\hat{Q}^* & -\sqrt{2}\hat{R} & \hat{P}+\Delta & 0 \\ \sqrt{2}\hat{R}^* & \sqrt{2}\hat{Q}^* & \sqrt{\frac{3}{2}}\hat{S}^* & -\frac{1}{\sqrt{2}}\hat{S} & 0 & \hat{P}+\Delta \end{pmatrix} + (\hat{V}_h + e\vec{r}\vec{F})I, \tag{A1}$$

where $\hat{V}_h$ is the confinement potential, $\vec{r}$ is the hole position vector, and **I** is the identity matrix, $\Delta = 300$ meV is taken for the spin-orbit shift. The operators appearing in this Hamiltonian, which were not defined above are

$$\hat{P} = \frac{\gamma_1}{2}(\hat{p}_x^2 + \hat{p}_y^2 + \hat{p}_z^2), \tag{A2}$$

$$\hat{Q} = \frac{\gamma_2}{2}(\hat{p}_x^2 + \hat{p}_y^2 - 2\hat{p}_z^2). \tag{A3}$$

In the evaluation of the z-component Hamiltonian (8) for the split-off hole band we use the effective mass $m_{SO}^* = 1/\gamma_1$.

[1] G. S. Solomon, J. A. Trezza, A. F. Marshall, and J. S. Harris, Jr., Phys. Rev. Lett. **76**, 952 (1996); N. N. Ledentsov, V. A. Shchukin, M. Grundmann, N. Kirstaedter, J. Böhrer, O. Schmidt, D. Bimberg, V. M. Ustinov, A. Yu. Egorov, A. E. Zhukov, P. S. Kopév, S. V. Zaitsev, N. Yu. Gordeev, Zh. I. Alferov, A. I. Borovkov, A. O. Kosogov, S. S. Ruvimov, P. Werner, U. Gösele, and J. Heydenreich, Phys. Rev. B **54**, 8743 (1996).

[2] S. Fafard, M. Spanner, J. P. McCaffrey, and Z. R. Wasilewski, Appl. Phys. Lett. **76**, 2268 (2000).

[3] H. J. Krenner, M. Sabathil, E. C. Clark, A. Kress, D. Schuh, M. Bichler, G. Abstreiter, and J. J. Finley, Phys. Rev. Lett. **94**, 057402 (2005).

[4] E. A. Stinaff, M. Scheibner, A. S. Bracker, I. V. Pomonarev, V. L. Korenev, M. E. Ware, M. F. Doty, T. L. Reinecke, and D. Gammon, Science **311**, 636 (2006).

[5] For a review, see M. Scheibner, A. S. Bracker, D. Kim, and D. Gammon, Solid State Commun. **149**, 1427 (2009).

[6] The heavy hole contribution to the ground state is usually larger than 90%, which is due to small height of self-assembled quantum dots, see for instance A. Schliwa, M. Winkelnkemper, and D. Bimberg, Phys. Rev. B **76**, 205324 (2007).

[7] B. Szafran, T. Chwiej, F. M. Peeters, S. Bednarek, J. Adamowski, and B. Partoens, Phys. Rev. B **71**, 205316 (2005).

[8] H. J. Krenner, E. C. Clark, T. Nakaoka, M. Bichler, C. Scheurer, G. Abstreiter, and J. J. Finley, Phys. Rev. Lett. **97**, 076403 (2006).

[9] J. I. Climente, M. Korkusiński, G. Goldoni, and P. Hawrylak, Phys. Rev. B **78**, 115323 (2008).

[10] J. M. Luttinger and W. Kohn, Phys. Rev. **97**, 869 (1955).

[11] M. F. Doty, J. I. Climente, M. Korkusiński, M. Scheibner, A. S. Bracker, P. Hawrylak, and D. Gammon, Phys. Rev. Lett. **102**, 047401 (2009).

[12] J. I. Climente, Appl. Phys. Lett. **93**, 223109 (2008).

[13] M. Scheibner, M. F. Doty, I. V. Ponomarev, A. S. Bracker, E. A. Stinaff, V. L. Korenev, T. L. Reinecke, and D. Gammon, Phys. Rev. B **75**, 245318 (2007).

[14] A. S. Bracker, M. Scheibner, M. F. Doty, E. A. Stinaff, I. V. Pomonarev, J. C. Kim, L. J. Whitman, T. L. Reinecke, and D. Gammon, Appl. Phys. Lett. **89**, 233110 (2006).

[15] M. Scheibner, M. Yakes, A. S. Bracker, I. V. Ponomarev, M. F. Doty, C. S. Hellberg, L. J. Whitman, T. L. Reinecke, and D. Gammon, Nat. Phys. **4**, 291 (2008).

[16] L. G. C. Rego, P. Hawrylak, J. A. Brum, and A. Wójs, Phys. Rev. B **55**, 15694 (1997).

[17] I. Vurgaftman, J. R. Meyer, and L. R. Ram-Mohan, J. Appl. Phys. **89**, 5815 (2001).

[18] M. Stopa and C. M. Marcus, Nano Lett. **8**, 1778 (2008).

[19] In formula (17) the integration over the angle and summation over the hole bands and electron spin directions gives a factor $2\pi\delta_{0,(m_z'-m_z+l'-l)}\delta_{j_z,j_z'}\delta_{\sigma',\sigma'}$, where δ is the Kronecker delta.

[20] V. S. Popov, Phys. Ät. Nucl. **68**, 717 (2004).

[21] S. L. Chuang, *Physics of Optoelectronic Devices* (Wiley, New York, 1995).